AUTOMATED SEGMENTATION OF SURFACE SOIL MOISTURE FROM LANDSAT TM DATA

Joseph Bosworth, Takashi Koshimizu, Scott T. Acton

Oklahoma Imaging Laboratory
School of Electrical and Computer Engineering, Oklahoma State University
Stillwater, Oklahoma 74078 U.S.A.
http://spiff.ecen.okstate.edu/spac/oil/imagelab.htm

ABSTRACT

This study demonstrates a method for satellite remote sensing of surface soil moisture and the automated segmentation of the acquired imagery. The remote sensing method exploits the relationship between surface radiant temperature, vegetation cover, and surface soil moisture. The segmentation process employs a watershed algorithm applied within a morphological image pyramid. This multi-resolution approach compares favorably to fixed-resolution techniques both in computational cost and feature scalability. Applications of both the remote sensing method and image segmentation technique are demonstrated for a Landsat TM image of southwestern Oklahoma.

I. INTRODUCTION

The potential for soil moisture (SM) measurement by satellite has been recognized for the past two decades [5]. Only recently, however, have techniques been developed for standardizing the conversion of satellite spectral measurements to surface SM. Specifically, the "triangle method" [4] uses the relationship between the surface radiant temperature and the vegetation index in estimating surface SM. In our study, we have attempted to automate the segmentation of the raw SM image using a multi-resolution watershed pyramid.

II. REMOTE SENSING OF SOIL MOISTURE

A. Satellite Data

For our investigation, we have selected a 185x170 km region of southwest Oklahoma, one of the world's best instrumented and most studied areas for SM, hydrology, and meteorology. The region contains the ARS Micronet (in the Little Washita basin) and several Oklahoma Mesonet sites, which constantly measure meteorological and surface parameters, including (recently) soil moisture. This selection allows the greatest potential for ground truth measurements and comparison with other studies.

The satellite data used in the example provided in this paper was acquired from the Landsat TM on a nearly cloudless summer day (July 25, 1997). Red, near-infrared, and thermal infrared spectral bands were used in determining vegetation index and surface radiant temperature. These spectral bands have a spatial resolution of 30 meters, with the exception of the thermal band, which has a resolution of 120 meters.

B. The Triangle Method

The triangle method assumes that surface radiant temperature depends primarily on vegetation cover and SM. During the daytime, bare soil is heated by solar radiation by an amount dependent upon SM (diurnal heat capacity). Thus, the radiant temperature of the soil is a measure of the (surface) SM content. In contrast, vegetation has the ability to regulate temperature (by transpiration) and therefore mask any information about the SM underneath, unless the vegetation experiences water stress [2]. Thus, in the absence of water stress, the surface radiant temperature is affected by the amount of bare soil and its SM content.

The quantity of bare soil within a given pixel is indicated by the Normalized Differential Vegetation Index (NDVI), defined in terms of Landsat TM spectral reflectance data (R) as

$$NDVI = \frac{R_{\text{nearinfrared}} - R_{\text{red}}}{R_{\text{nearinfrared}} + R_{\text{red}}}. \quad (1)$$

The NDVI ranges between near 0.8 for completely vegetated areas to 0.05 for completely bare soil, and near –0.5 for bodies of water.

Surface radiant temperature (SRT) is determined by the thermal infrared band of Landsat TM (wavelength 10.4-12.5 μm). In contrast to NDVI, the local range of SRT varies significantly within the 185x170 km image, due to surface and meteorological conditions (air temperature, humidity, solar radiation, wind, etc.). It is possible to estimate corrections for many of these factors

This work was supported by the National Aeronautics and Space Administration under EPSCOR grant NCC5-171.

using additional meteorological data and models. However, in our study we have attempted to avoid meteorological inhomogeneity by analyzing smaller regions of 12x12 km, within which only the *relative* SRT is used in determining SM.

The "triangle method" derives its name from the shape of the "scatterplot" showing the occurrence of SRT on the horizontal axis and NDVI on the vertical axis. The scatterplot for the 12x12 km subimage used in this paper is shown in Fig. 1.

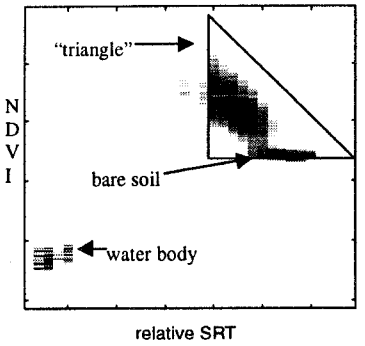

Fig. 1 Scatterplot of NDVI vs. SRT

The triangular shape of the scatterplot can be interpreted as follows: The more vegetated an area (higher NDVI), the lower the temperature. However, there is some spread in temperature due to differing quantities of soil moisture. Therefore, for a given NDVI, *relatively* high temperatures correspond to low amounts of soil moisture. The triangle method assumes that soil moisture varies from completely dry (right edge of the triangle) to completely saturated with moisture (left edge).

In theory, the apex of the triangle corresponds to total vegetation (no bare soil), at which point no variation in temperature should be observed. In practice, the apex is chosen at total vegetation and at the temperature that includes the most pixels within the triangle. The base of the triangle corresponds to bare soil, and can easily be distinguished by its low NDVI.

Within the triangle, lines of equal SM, called "isopleths," can be calculated by a boundary layer model using surface and meteorological parameters. With the goal of automating the process, we have instead chosen the isopleths to be linear and equally spaced in slope. (Pixels outside the triangle were assigned the value of the nearest isopleth.) Fig. 2 shows the NDVI of a 12x12 km area, and Fig. 3 shows the SRT image. The lighter pixels in Figs. 2 and 3 represent higher values of NDVI and lower SRT, respectively. The soil moisture image obtained by the triangle method is shown in Fig. 4, with darker pixels representing higher SM.

C. Assessment of the Triangle Method

Research is ongoing regarding the existence of a "universal triangle" with isopleths that correspond to *absolute* values of surface soil moisture [4]. In our present research, we are attempting to incorporate meso-scale ground measurements into the identification of absolute soil moisture isopleths.

As a consequence of using optical remote sensing, the SM data obtained by the triangle method allow measurement at a thin surface layer (less than 5 mm in depth). During rapid drying, this surface layer becomes decoupled with deeper soil layers [1]. Therefore, the triangle method alone cannot give an accurate measure of the *vertical* SM profile. However, in conjunction with microwave SM techniques, the method may aid the measurement of important surface soil properties and/or vegetation water stress.

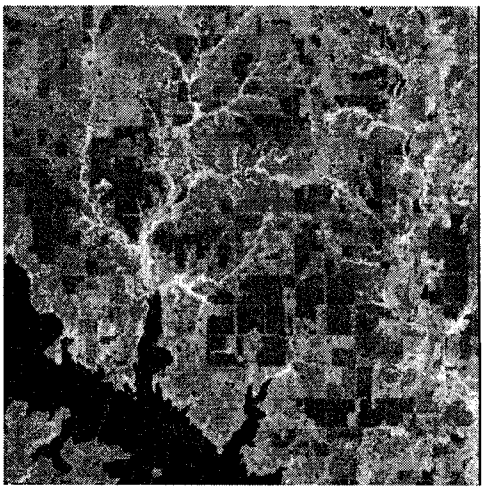

Fig. 2 NDVI

Fig. 3 Surface Radiant Temperature

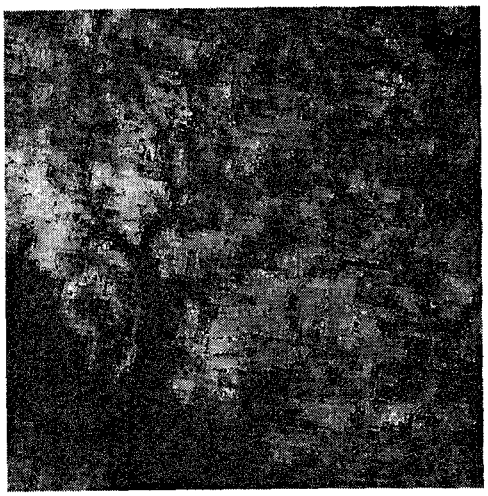

Fig. 4 Original Soil Moisture Image

III. IMAGE SEGMENTATION

A. The Watershed Algorithm

Image segmentation is the process of dividing an image into homogeneous sub-regions. Our objective is to provide an unsupervised segmentation of the SM image. There are a variety of edge detection methods useful for segmentation. In this study, we focus on the *watershed* technique as applied to the segmentation of our SM image [3]. The watershed algorithm is advantageous because the resulting edges are thin and continuous, and the boundaries are closed. First, we explain the fixed-resolution watershed algorithm and then we extend the concept to the multi-resolution watershed pyramid.

The concept of the watershed comes from topography. The *gradient magnitude* of the image is considered as a topographic surface, where low gradient values are represented as "catchment basins." High gradient values are "ridges," forming the watershed boundaries that correspond to edges in the actual image.

A "minimum-following" algorithm can be utilized to link each pixel location to the location of the catchment basin into which it drains. Because each pixel location must have a unique local minimum in gradient magnitude, the gradient magnitude image is slightly blurred by a Gaussian kernel:

$$\mathbf{B} = \mathbf{G} * |\nabla \mathbf{I}| \qquad (2)$$

where $\mathbf{I}$ is original image, $\mathbf{G}$ is the Gaussian kernel and $\nabla \mathbf{I}$ is gradient of $\mathbf{I}$. The next step is to find the local minima of $\mathbf{B}$. These local minima represent the catchment basins of the gradient magnitude image, and they are each labeled by a unique number for the identification.

The last step is to group catchment basins of the same label together. This process is defined as

$$\mathbf{W} = \mathbf{WS}(\mathbf{B}). \qquad (3)$$

After all of the watersheds have been labeled, the edge map is computed by locating the boundaries between watersheds.

Unfortunately, the above process gives a heavily over-segmented image. Typically, a region combination technique is applied in an attempt to reduce the number of regions in the segmentation.

B. The Watershed Pyramid

Despite the addition of the region combination technique to the fixed-resolution watershed, the image remains over-segmented. This difficulty can be avoided (and computation time greatly reduced) by utilizing the scalable segmentation produced by a morphological image pyramid [3]. In this technique, the watershed algorithm is applied to a coarse level of the image pyramid, then the edges are propagated down to the finer layers of the pyramid.

The pyramid is created by a succession of filtering and sub-sampling as follow. Level L is given as

$$\mathbf{I}_L = [(\mathbf{I}_{L-1} \circ \mathbf{K}) \bullet \mathbf{K}] \downarrow 2 \quad L=0,1,\ldots, \text{n}. \qquad (4)$$

Here, $\mathbf{I}_0$ is the original image and $[.]\downarrow 2$ represents down sampling by a factor of two. $\mathbf{I}_L$ is referred to as the "parent" level of $\mathbf{I}_{L-1}$, the "child". With one-of-two down-sampling in both dimensions, each parent has four children. $(\mathbf{I} \circ \mathbf{K})$ and $(\mathbf{I} \bullet \mathbf{K})$ represent the morphological opening and closing by structuring element $\mathbf{K}$, respectively. In this process, the open-close operation was chosen because it produces reduced grayscale bias as compared to the individual open or close operation [6]. The morphological filter is superior to linear filters (as used in the Gaussian pyramid) in terms of edge localization and feature preservation.

The watershed algorithm is applied on a coarse level gradient magnitude image $|\nabla \mathbf{I}_L|$, and the resultant segmentation is denoted by $\mathbf{W}_L$. The gradient values of the child level $\mathbf{W}_{L-1}$ are created by linking each pixel to one in the parent level $\mathbf{W}_L$. Hence,

$$\mathbf{W}_{L-1}(i_o, j_o) = \begin{cases} \mathbf{W}_L(i,j) & \text{if } |\nabla \mathbf{W}_L(i,j)| = 0 \\ \text{undefined if } |\nabla \mathbf{W}_L(i,j)| > 0 \end{cases} \qquad (5)$$

where (i_o, j_o) is a child pixel at level L-1 for parent element (i,j) at level L.

In (5), if $|\nabla \mathbf{W}_L(i,j)| = 0$, the label of the children of pixel (i, j) is assigned to be that of the parent. The final step in linking level L-1 to level L is the application of the (fixed-resolution) watershed algorithm on the pixels of $\mathbf{W}_{L-1}(i, j)$ with undefined links (for children which have edge pixels as parents).

The linking process continues level by level, terminating with the level corresponding to the original image resolution.

C. Results

Fig. 4 depicts the result of applying the fixed-resolution watershed segmentation to the raw soil moisture image, and Fig. 5 gives the resultant edge map. Although connected and thin contours are provided, the image is clearly over-segmented. The segmentation regions and edge maps from the multi-resolution watershed technique are shown in Figs. 6 through 11. The root level was varied from 2 to 4 in this example in order to demonstrate the scalability of the segmentation. Table summarizes the results of computation time and the number of segmented regions produced by varying the root level.

For our 512x512 image, the fixed-resolution method took more than 16 minutes to process, while the multi-resolution watershed approach required only 15 seconds on a Sun Ultra 1/170 workstation. Through the selection of different root levels, the multi-resolution watershed pyramid produced a scalable segmentation, varying from coarse to fine. This scalability gives the multi-resolution approach a distinct advantage over the fixed-resolution approach.

From these results it is clear that the multi-resolution watershed pyramid is capable of providing an appropriately scaled segmentation with over an order of magnitude improvement in computation time over the fixed-resolution watershed method.

Table	Root Level	Computation Time	Number of Regions
Fixed-Resolution	0	16.5 min	1075
Multi-Resolution	2	15 sec	413
Multi-Resolution	3	15 sec	109
Multi-Resolution	4	15 sec	31

REFERENCES

[1] W.J. Capehart, and T.N. Carlson, "Decoupling of surface and near-surface soil water content: A remote sensing perspective," *Water Resources Research*, vol. 33, no. 6, pp. 1383-1395, Jun. 1997.

[2] T.N. Carlson, and R.R. Gillies, "Remote sensing of soil moisture over vegetation. Sensitivity and limitations of the infrared temperature method," *20th Conf. Agricultural and Forestry Meteorology*, Salt Lake City, UT, Amer. Meteor. Soc., pp. 214-217, 1991.

[3] J.M. Gauch, and S.M. Pizer, "Multiresolution Analysis of Ridges and Valleys in Gray-Scale Images," *IEEE Transaction on Pattern Analysis and Machine Intelligence*, vol. 15, no. 6, 1993.

[4] R.R. Gillies, and T.N. Carlson, "Thermal Remote Sensing of Surface Soil Water Content with Partial Vegetation Cover for Incorporation into Climate Models," *J. Appl. Meteor.*, vol. 34, pp. 745-756, Apr. 1995.

[5] J.C. Price, "The Potential of Remotely Sensed Thermal Infrared Data to Infer Surface Soil Moisture and Evaporation," *Water Resour. Res.*, vol. 16, pp. 787-795, Aug. 1980.

[6] A. Wright, and S.T. Acton, "Watershed pyramids for edge detection," *Proc. of the IEEE Int. Conf. on Image Processing*, Santa Barbara, Ca., Oct. 26-29, 1997.

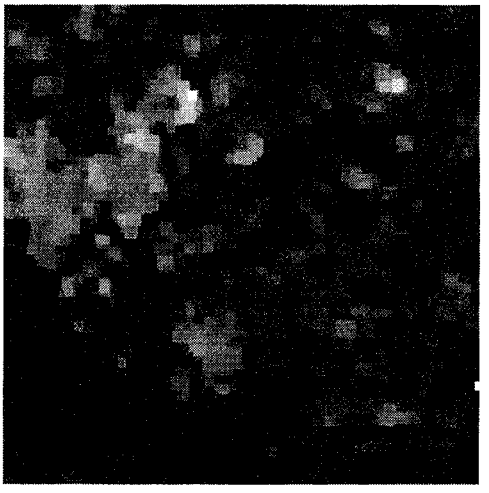

Fig. 4 Fixed-Resolution Image

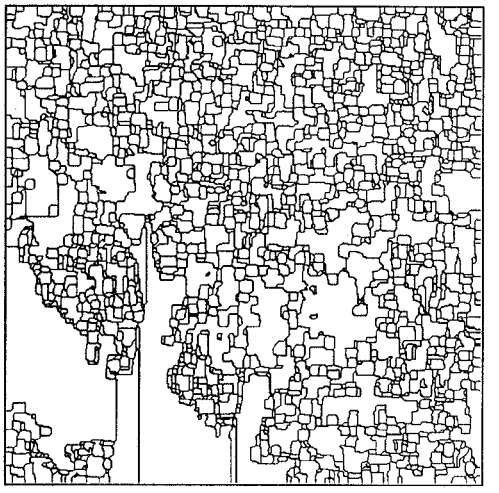

Fig. 5 Fixed-Resolution Edge Map

Fig. 6 Multi-Resolution Image (Root = 2)

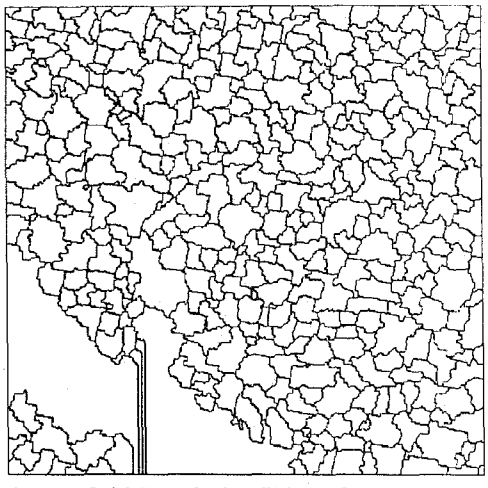

Fig. 7 Multi-Resolution Edge Map (Root = 2)

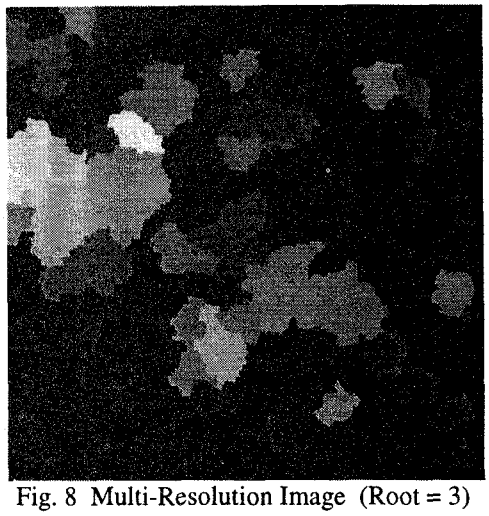

Fig. 8 Multi-Resolution Image (Root = 3)

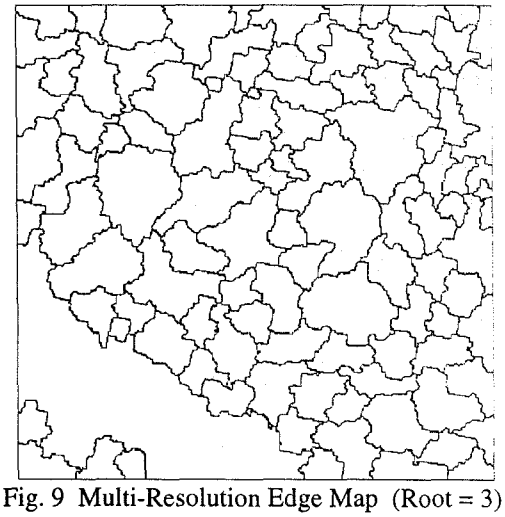

Fig. 9 Multi-Resolution Edge Map (Root = 3)

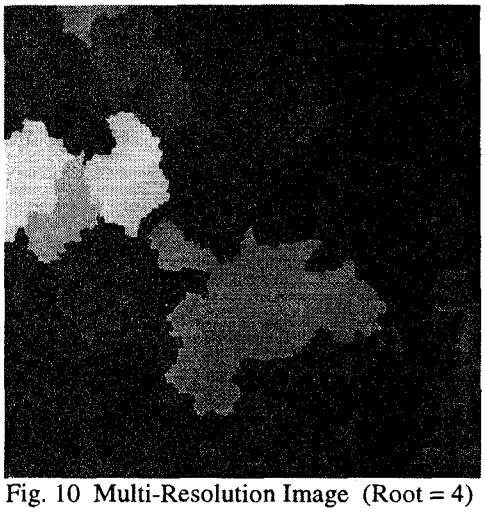

Fig. 10 Multi-Resolution Image (Root = 4)

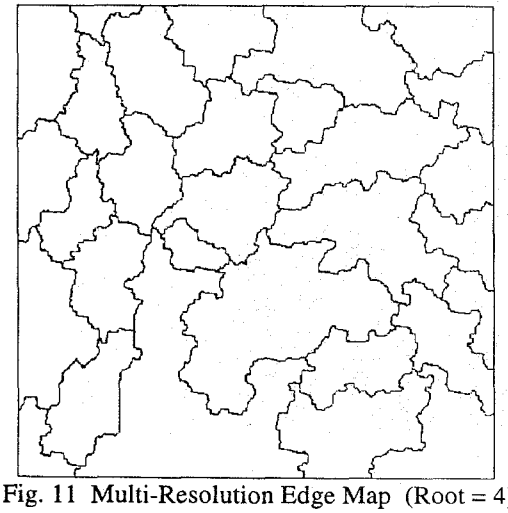

Fig. 11 Multi-Resolution Edge Map (Root = 4)